DFT Mechanistic Proposal of the Ruthenium Porphyrin-Catalyzed Allylic Amination by Organic Azides

Gabriele Manca,*[,†] Emma Gallo,*[,‡] Daniela Intrieri,[‡] and Carlo Mealli[†]

[†]Istituto di Chimica dei Composti OrganoMetallici (ICCOM-CNR), Via Madonna del Piano 10, I-50019 Sesto Fiorentino Florence, Italy

[‡]Dipartimento di Chimica, Università degli Studi di Milano, Via C. Golgi 19, I-20133 Milan, Italy

S *Supporting Information*

ABSTRACT: A DFT-based theoretical analysis describes the allylic amination of cyclohexene by $3,5(CF_3)_2$phenylazide catalyzed by $[Ru](CO)$ ($[Ru]= Ru(TPP)$, TPP = dianion of tetraphenylporphyrin). The activation of an azide molecule (RN_3) at the free ruthenium coordination site allows the formation of a monoimido complex $[Ru](NR)(CO)$ with the eco-friendly dismissal of a N_2 molecule. The monoimido complex can undergo a singlet→triplet interconversion to confer a diradical character to the RN ligand. Hence, the activation of the allylic C−H bond of cyclohexene (C_6H_{10}) occurs through a C−H···N interaction over the transition state. The formation of the desired allylic amine follows a "rebound"

mechanism in which the nitrogen and carbon atom radicals couple to yield the organic product. The release of the allylic amine restores the initial $[Ru](CO)$ complex and allows the catalytic cycle to resume by the activation of another azide molecule. On the singlet PES, the CO ligand may however be eliminated from the monoimido complex $[Ru](NR)(CO)_S$, opening the way to an alternative catalytic cycle which also leads to allylic amine through comparable key steps. A second azide molecule occupies the vacant coordination site of $[Ru](NR)_S$ to form the bis-imido complex $Ru(TPP)(NR)_2$, which is also prone to the intersystem crossing with the consequent C−H radical activation. The process continues until the azide reactant is present. The interconnected cycles have similarly high exergonic balances. Important electronic aspects are highlighted, also concerning the formation of experimentally observed byproducts.

KEYWORDS: *organic azides, ruthenium porphyrin catalysts, C−H aminations, radical reactivity, DFT energy profiles*
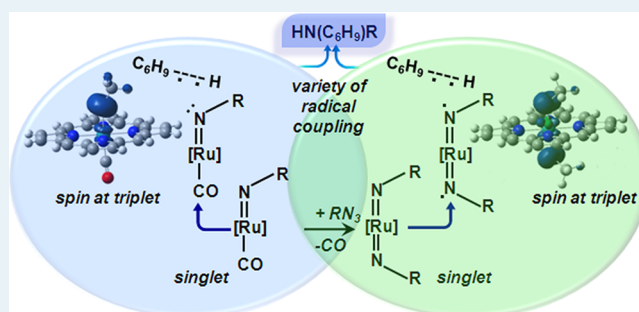
■ INTRODUCTION

The insertion of an "RN" moiety into an organic skeleton is a process of fundamental interest affording aza-derivatives with intriguing pharmaceutical and/or biologic properties.[1−5] Among available "RN" sources, organic azides (RN_3) are eco-friendly and efficient aminating reagents, since the only byproduct is molecular nitrogen.[6−8] Therefore, the research on the topic has strongly increased in the past decade.[9−11] Among transition metal catalysts able to transfer a nitrene functionality into an organic skeleton,[10,12−15] metal porphyrins present excellent activity, which is often associated with high chemio-, stereo-, and enantioselectivity.[16−18] The studies on the catalytic efficiency of these complexes in the direct and low cost amination of hydrocarbon C−H bonds[16,17,19] have been hence aimed to understand the reaction mechanisms, based on which the experimental procedures can be optimized.[20−29]

In the past few years, some of us reported a mechanistic investigation of the ruthenium porphyrin-catalyzed amination of allylic C−H bonds by aryl azides (ArN_3). A catalytic mechanism was suggested from the nature of isolated ruthenium intermediates and kinetic and spectroscopic studies.[20] Data indicated two coexisting catalytic cycles

involving the complex $Ru(TPP)(CO)$ (TPP = dianion of tetraphenyl porphyrin), which is the precursor of the oxidized species $Ru(TPP)(NAr)(CO)$ and $Ru(TPP)(NAr)_2$ (Ar = $3,5(CF_3)_2C_6H_3$).[30] While $Ru(TPP)(NAr)(CO)$ has never been isolated, the bis-imido complex $Ru(TPP)(NAr)_2$ was fully characterized and independently found to have good catalytic activity in the amination of allylic C−H bonds. This raises the hypothesis that the two imido complexes, which both support an independent catalytic cycle, can be strictly interconnected.

This paper presents a DFT computational investigation on the allylic amination of cyclohexene, which sheds light on the activation of aryl azides by ruthenium porphyrins toward allylic C−H bonds. Our parent model is $[Ru](CO)$ (where $[Ru]$ is the $Ru(TPP)$ planar moiety with H in place of Ph substituents), and methyl azide CH_3N_3 was preferred to the aryl analogues used in the experiments for their high stability/reactivity relationship.[20] The approximations sped up the calculations and

facilitated general electronic interpretations such as an evident radical character of the chemistry. In some cases, the experimentally employed $3,5(CF_3)_2C_6H_3N_3$ azide was modeled to provide a more quantitative evaluation of key catalytic steps. In particular, it was found that not only the energy barriers are about 25−30% lower with respect to those calculated by employing CH_3N_3 but also the access to some key intermediate is more energetic.

■ RESULTS AND DISCUSSION

Synthetic Studies. The kinetic and spectroscopic data in our previous papers[20,30] suggested the existence of the two catalytic mechanisms highlighted in Scheme 1. A particular relevance had the very reactive species $[Ru](NAr)(CO)$, **C**, obtained upon the activation of one aryl azide molecule over $[Ru](CO)$.

Scheme 1. Proposed Mechanism for the $[Ru](CO)$-Catalyzed Allylic Amination of Cyclohexene
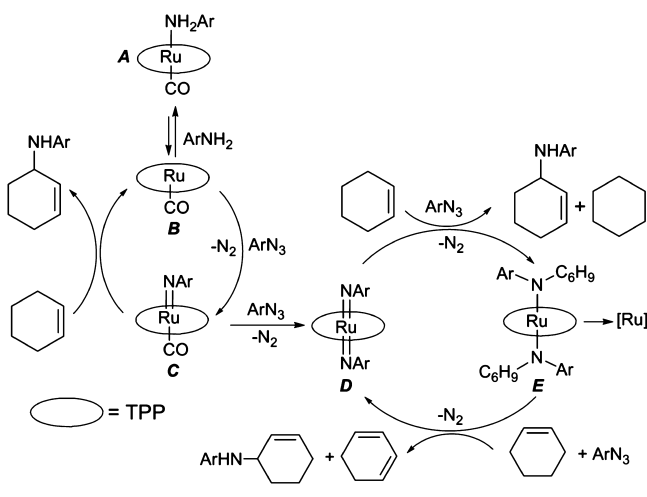
To favor the trapping and characterization of $[Ru](NAr)$-(CO), the allylic amination of cyclohexene was attempted in the presence of $4(^tBu)C_6H_4N_3$. The low oxidation power of this azide could prevent the formation of the bis-imido complex **D**, usually obtained by employing more oxidant azides such as $3,5(CF_3)_2C_6H_3N_3$. As expected,[20] the reaction did not occur at room temperature, but at 80 °C it leads to the $[Ru^{II}](Ar'NH_2)$-(CO) amino complex, **A** ($Ar' = 4(^tBu)C_6H_4$). As already discussed,[20] the probable precursor of **A** is the monoimido species $[Ru^{IV}](NAr')(CO)$, which can be easily involved in hydrogen abstraction reactions. It is noteworthy that the similar amino complex $[Ru](ArNH_2)(CO)$ was also obtained at 0 °C by irradiating the reaction mixture of $[Ru](CO)$ and $3,5$-$(CF_3)_2C_6H_3N_3$ with a halogen lamp. Then, the reaction between the isolated $[Ru](NAr)_2$[20] and $[Ru](CO)$ was attempted to study the oxidation power of the ruthenium(VI) complex. The expected disproportion reaction to yield $[Ru](NAr)(CO)$ did not occur even at relatively high temperatures or under a CO atmosphere.

The following computational analysis provides a useful validation of various aspects of Scheme 1 and highlights important species which govern the catalytic reactivity. Additionally, this theoretical study sheds light on the connection of the two catalytic cycles (Scheme 1) which are both active in the experimental chemistry.

DFT Computational Studies of the Catalytic Mechanisms. The B97D functional[31] was preferred to the standard B3LYP one[32] for including dispersion forces. These can play an important role in systems where a delocalized metal-porphyrin planar unit weakly interacts with apically coordinated ligands. In any case, the different response of the two functionals will be occasionally pointed out, in particular for important steps of the intersystem crossing.

Activation of the First Azide Molecule and Formation of the $16e^-$ $[Ru](NCH_3)(CO)$ Species. The optimized $16e^-$ model $[Ru](CO)$ is a minimum (Figure S1), although in several X-ray structures[33] the moiety is weakly coordinated by a sixth ligand (e.g., an H_2O solvent molecule[34]). The closest experimental evidence of an almost pure five-coordinated $[Ru](CO)$ complex is the adduct between $Ru^{II}(OEP)(CO)$ (OEP = dianion of octaethylporphyrin) and a C_{60} molecule.[35] The latter is only weakly coordinated to ruthenium through one 5:6 junction likely on account of extended dispersion forces involving the fullerene π system and the OEP periphery. Our optimized $[Ru](CO)$ model shows Ru−CO and Ru−N_{TPP} distances only 0.03 Å larger (1.78 and 2.07 Å, respectively) than those reported in the paper discussed above.[35]

Although an azide adduct of $[Ru](CO)$ was never experimentally identified, two alternative minima were optimized with the CH_3N_3 coordinating through either the N_α or N_γ atom (Figures 1 and S2, respectively). While the
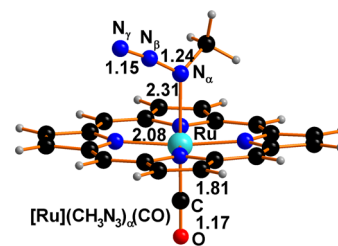

Figure 1. Optimized azide adduct $[Ru](CH_3N_3)_\alpha(CO)$.

former adduct $[Ru](CH_3N_3)_\alpha(CO)$ (Figure 1) is exergonic by -3.5 kcal mol^{-1}, the isomer $[Ru](CH_3N_3)_\gamma(CO)$ is disfavored ($+2.5$ kcal mol^{-1}) because the remote methyl substituent is uninvolved in dispersion interactions.

Previous theoretical studies (e.g., for nonporphyrin ruthenium complexes[36,37]) have exclusively addressed the azide N_α coordination, while the importance of the N_γ adduct was experimentally corroborated for a tantalum azide complex.[38] The latter evolves into a four-membered "TaN$_3$" ring, of which no "RuN$_3$" analogue could be computationally detected. For this reason, no further analysis of the reactivity through the azide γ coordination was pursued.

The azide coordination in the minimum $[Ru]$-$(CH_3N_3)_\alpha(CO)$, of which no experimental structural evidence has ever been reported, is rather weak. The dispersion forces used in our calculation clearly provide extra stabilization, since the large Ru−N_α distance of the 2.37 Å computed at the B3LYP level (see Figure S3)[32] is reduced to 2.31 Å. From previous experimental/theoretical studies, the Ni−S interaction, involving a Ni^I macrocycle and an apical thioethereal group, was found to become bonding only at low temperatures, being computationally attributed to dispersion forces.[39]

In the energy profile of Scheme 2, the formation of the azide adduct $[Ru](CH_3N_3)_\alpha(CO)$ allows subsequent access to the transition state $[Ru](CH_3N_3)(CO)_{TS}$ with a ΔG cost of $+26.8$

Scheme 2. Energy Profile for the Formation of Ru^{IV} Mono-Imido Species
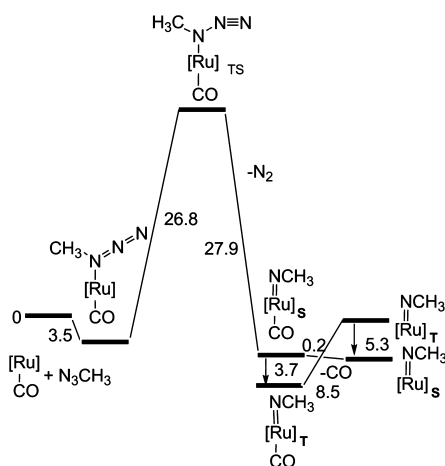
kcal mol^{-1}. This barrier is consistent with the 80 °C temperature required for the catalysis to proceed.

Since electron-withdrawing aryl substituents at the azide are known to favor the experimental reactivity,[40] we checked whether the barrier is lowered when the azide 3,5-$(CF_3)_2C_6H_3N_3$ is used as a substrate (see Scheme S1). A path analogous to that reported in Scheme 2 was computed, and the recorded lower barrier of +20.4 kcal mol^{-1} confirms the better catalytic performance of azides bearing electron withdrawing substituents on the aryl moiety. It is worth mentioning that similar barriers were generally computed for the activation of an organic azide over a cobalt porphyrin complex with no *trans* CO ligand.[22,21,24] The system in question can be related to ours, because the metal axial orbital (mainly z^2), which in our case contributes to the Ru–CO σ bond, for Co(II) stands alone as singly occupied without interfering with the azide activation. Figure 2 shows structural
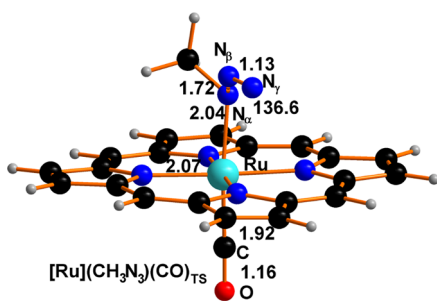

Figure 2. Optimized singlet structure of $[Ru](CH_3N_3)(CO)_{TS}$.

details of the $[Ru](CH_3N_3)(CO)_{TS}$ optimized structure, where an almost unperturbed N_2 molecule is ready to leave. In fact, the $N_\beta–N_\gamma$ distance is relatively short (1.13 Å), while the $N_\alpha–N_\beta$ one is 1.72 Å long and the N_3 unit has lost its linearity ($N_\alpha–N_\beta–N_\gamma$ angle = 136.6°). In the initial adduct $[Ru]-(CH_3N_3)_\alpha(CO)$ (Figure 1), both the $N_\alpha–N_\beta$ and $N_\beta–N_\gamma$ distances are comparably short (1.24 and 1.15 Å, respectively), consistent with two orthogonal π delocalized interactions somewhat related to those of unsubstituted 16e$^-$ linear triatomics (see below).

At $[Ru](CH_3N_3)(CO)_{TS}$, the Ru–N_α linkage is strengthened from 2.31 to 2.04 Å, while the *trans* Ru-CO bond elongates from 1.81 to 1.92 Å, hence a reduced Ru→CO back-donation.

An IRC procedure beyond TS indicates that the N_2 elimination is stabilizing (−27.9 kcal mol^{-1} in Scheme 2) and leads to the complex $[Ru](NCH_3)(CO)_S$ with a formal Ru^{IV} metal and an imido dianionic ligand. Importantly, the same compound also exists as the triplet $[Ru](NCH_3)(CO)_T$, which is more stable by −3.7 kcal mol^{-1}. Figure 3 shows the spin isomers with a consistent primary octahedral structure but some different geometrical parameters.
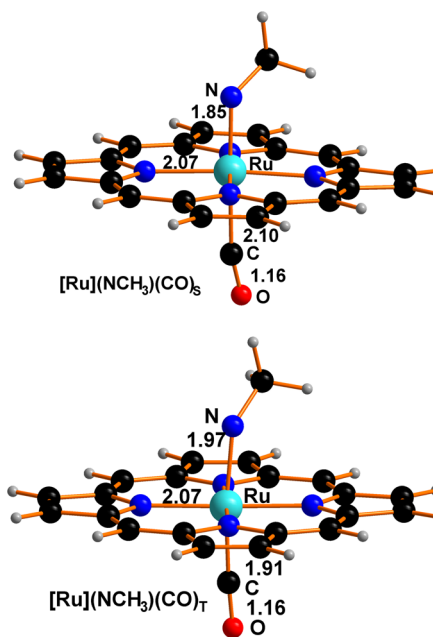

Figure 3. Optimized structures of $[Ru](NCH_3)(CO)_S$ and $[Ru]-(NCH_3)(CO)_T$.

In particular, the Ru–N_α and Ru–CO distances follow opposite trends. The imido ligand in the singlet isomer is more strongly bound (1.85 vs 1.97 Å), while the CO one is more loose (2.10 vs 1.91 Å) as it had almost departed. Indeed, the attainment of the five-coordinated derivative $[Ru](NCH_3)_S$ (Figure S4a) has practically no cost (−0.2 kcal mol^{-1}), while in the triplet the CO loss, to give $[Ru](NCH_3)_T$ (Figure S4b), costs +8.5 kcal mol^{-1}.

At this point, we focused on the timeliness of the spin crossings and its implications for the catalytic reactivity. First of all, attempts to optimize the triplet TS analogous to $[Ru](CH_3N_3)(CO)_{TS}$ failed, thus excluding the possibility of the intersystem crossing before the azide activation. For any couple of spin isomers in Scheme 2, the ΔG gap and eventually the stability order depends on the used DFT functional. To check the point, the B3LYP and BP86[41] functionals (besides B97D) were tested, confirming that in any case the triplet is more favored for the octahedral species but disfavored for the five-coordinated one. The largest ΔG difference does not exceed 5 kcal mol^{-1}. To elucidate the evolution of the spin crossing and its energy cost (Minimum Energy Crossing Point, MECP[42]), we combined in Figure 4 the B97D relaxed scans of both $[Ru](NCH_3)(CO)_S$ and $[Ru](NCH_3)(CO)_T$ species upon the Ru–CO distance elongation (from 1.8 to 2.6 Å), which seems to be a major governing parameter for spin crossing. The right side of the picture implicitly corresponds to the behavior of the five-coordinated complexes $[Ru](NCH_3)_S$ and $[Ru](NCH_3)_T$, since the Ru–CO distance of 2.6 Å is
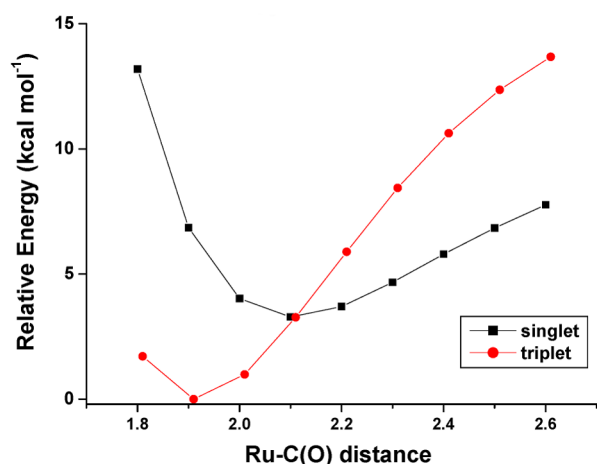
Figure 4. Singlet/triplet relaxed scans at the B97D level for the Ru–CO elongation in octahedral structures of type [Ru](NCH$_3$)(CO) (see Figure 3).

almost nonbonding. It appears that the triplet is stabilized at short Ru–CO distances, while the singlet is favored beyond the crossing point of ~2.1 Å. Since the intersection of the curves coincides with the minimum of the singlet PES, no extra energy cost has to be accounted for the spin crossover (MECP = 0).[42]

Electronic Aspects of the Azide Activation. The triplet [Ru](NCH$_3$)(CO)$_T$ is relevant for promoting radical reactivity. In fact, the unpaired spins do not exclusively concern the metal but also the imido nitrogen atom and possibly the delocalized TPP π system as suggested by other authors.[26] Significant spin localization at the NCH$_3$ moiety can determine its radical character, hence trigger the C–H homolysis at an hydrocarbon substrate with the subsequent formation of N–H and N–C bonds in the allylic amine product. The N$_2$ departure over the singlet state of [Ru](CH$_3$N$_3$)(CO) implies an oxidative addition process with the concomitant formation of a formal NCH$_3^{2-}$ dianion and a Ru^{IV} metal center. In a possible intermediate, the N$_\alpha$–N$_\beta$ cleavage may be promoted by its σ^* population at the expense of d$_\pi$ metal electrons, but no evidence of the azide dihapto coordination has ever been found. It is important to underline that the metal mitigates the activation process which can be even explosive in the case of the free methyl azide.[8] The different behavior can be explained in MO terms. In fact, Scheme 3a suggests that the two orthogonal and delocalized π levels of an isolated CH$_3$N$_3$ molecule compare with classical 16e$^-$ triatomics (e.g., CO$_2$) with some orbital reorientation due to the bent CH$_3$–N

Scheme 3. Electronic Underpinnings of the RN$_3$ Activation
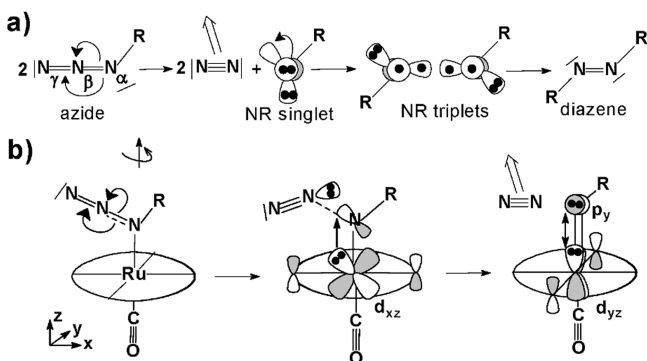
linkage. After the N$_2$ departure, the N$_\alpha$ p$_\pi$ orbital, in the plane of the Ru–N and R–N vectors, is a formal sp^2 vacant hybrid, which lies close in energy to the orthogonal and filled p$_\pi$ orbital. This allows the NCH$_3$ conversion into a nitrene diradical, which can dimerize to yield the experimentally observed CH$_3$N=NCH$_3$ diazene with the high exergonic balance of −105.2 kcal mol^{-1}.[43]

Scheme 3b illustrates the azide orbital evolution in the metal complex upon the N$_2$ departure. Some d$_\pi$ metal back-donation takes place from d$_{xz}$ into the N p$_\pi$ vacant orbital ("bent" p$_x$ or sp^2 component) and prevents the analogous electron unpairing, which occurs in the absence of the metal (Scheme 3a). Indeed, the transition state [Ru](CH$_3$N$_3$)(CO)$_{TS}$ only exists as a singlet, also characterized by a 4e$^-$ repulsion between the populated N-p$_y$ and Ru-d$_{yz}$ orbitals. Importantly, the LUMO, which descends from the N$_\alpha$–N$_\beta$ σ^* level, steeply stabilizes as N$_2$ separates. The crossing with the HOMO, which is in principle forbidden by the orthogonality of the two levels, becomes possible because of the lost azide planarity and the NCH$_3$ rotation about the Ru–N vector (the N$_{TPP}$RuNC torsion angle at [Ru](CH$_3$N$_3$)(CO)$_{TS}$ is 26°, as shown in Figure 2). In the singlet product [Ru](NCH$_3$)(CO)$_S$, the inverted HOMO/LUMO levels are again roughly orthogonal, with the LUMO having (p$_y$–d$_{yz}$)* nature (left side of Scheme 4). The energy separation is however small enough to allow the

Scheme 4. Frontier MO Distribution in [Ru](NCH$_3$)(CO)$_S$ and [Ru](NCH$_3$)(CO)$_T$
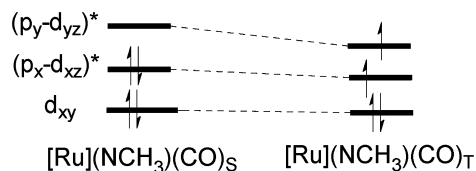
attainment of the triplet [Ru](NCH$_3$)(CO)$_T$ upon the unpairing of the (p$_x$–d$_{xz}$)* HOMO electrons (right side of Scheme 4). Also, it is worth remarking that the CO ligand is less strongly bound to the metal (hence, more easily lost) in the singlet than in the triplet (2.10 Å vs 1.91 Å as shown in Figure 3). In the former case, the metal π-back-donation from d$_{xz}$ into NCH$_3$ competes with that into CO, while in the triplet, two orthogonal interactions equally involve three electrons.

A plot of the spin density in the triplet [Ru](NCH$_3$)(CO)$_T$ is shown in Figure 5. Clearly, there is a larger concentration at the N$_\alpha$ atom than at the ruthenium one (1.59 vs. 0.31 e^2/
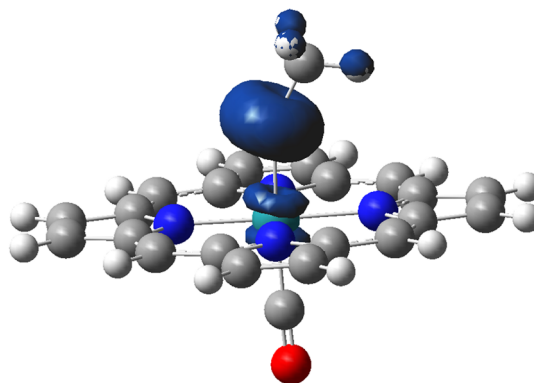

Figure 5. Spin density plot for [Ru](NCH$_3$)(CO)$_T$.

bohr^3). Therefore, a significant diradical character is attributed to the imido ligand. This may trigger a C−H homolytic dissociation of the organic substrate (e.g., cyclohexene) and eventually favors the amination chemistry depicted on the left side of Scheme 1.[20] An analogous singlet/triplet interplay for the bis-imido complex will be later indicated to support a diradical activity also in the cycle described on the right side of Scheme 1.

Activation of a Second Azide Molecule to Form [Ru](NCH$_3$)$_2$ Species. After the CO departure, both the five-coordinated spin isomers [Ru](NCH$_3$)$_S$ and [Ru](NCH$_3$)$_T$ possess a vacant σ hybrid to anchor another azide molecule. Both the adducts [Ru](NCH$_3$)(CH$_3$N$_3$)$_S$ and [Ru](NCH$_3$)-(CH$_3$N$_3$)$_T$ were optimized (Figure S5) with a similarly small exergonic balance (−0.3 and −1.9 kcal mol^1, respectively). The Ru−N$_\alpha$ linkages are similarly weak (2.35 and 2.34 Å, respectively), and the dispersion forces are mainly responsible for the azide addition as also corroborated by the comparison with B3LYP calculations. The subsequent azide activation is quite similar to that already described for the coordination of CH$_3$N$_3$ over [Ru](CO). In fact, the local structural features of the singlet TS species [Ru](NCH$_3$)(CH$_3$N$_3$)$_{TS}$ (Figure 6) are strictly comparable with those of [Ru](CH$_3$N$_3$)(CO)$_{TS}$ illustrated in Figure 2. Again, no analogous TS triplet could be optimized.
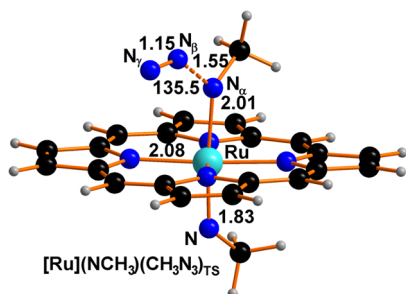

Figure 6. Optimized structure of [Ru](NCH$_3$)(CH$_3$N$_3$)$_{TS}$.

The energy profile in Scheme 5 shows that the TS barrier for the azide activation is approximately half of that in Scheme 2 (+14.0 vs +26.8 kcal mol^{-1}), while the subsequent bis-imido complex [Ru](NCH$_3$)$_{2\ S}$ is more stable than the corresponding monoimido one (−41.6 vs −27.9 kcal mol^{-1}). Finally, the triplet isomer [Ru](NCH$_3$)$_{2\ T}$ appears definitely more difficult to reach (+16.1 vs. +5.3 kcal mol^{-1}).

Scheme 5. Energy Profile for Activation of the Second Azide Molecule
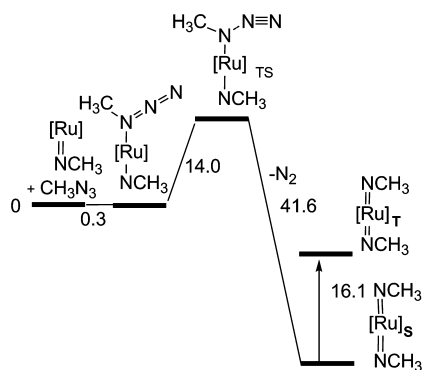
The strategy used for the plots in Figure 4 was repeated to study the intersystem crossing between [Ru](NCH$_3$)$_{2\ S}$ and [Ru](NCH$_3$)$_{2\ T}$ on varying one Ru−N$_\alpha$ distance. The singlet curve remains below the triplet one with an almost constant gap. Therefore, the triplet appears as an excited state, which lies +16.1 kcal mol^{-1} above the singlet. The ΔG gap is possibly overcome by heating and/or irradiating the reaction mixture. In fact, it was experimentally observed that the catalysis performed in the presence of bis-imido complexes is hindered at low temperatures and proceeds definitely better upon heating.

The isomers [Ru](NCH$_3$)$_{2\ S}$ and [Ru](NCH$_3$)$_{2\ T}$ are shown in Figure S6. The former and more stable compound is validated by the X-ray structure of [Ru](NAr)$_2$ with Ar = 3,5(CF$_3$)$_2$C$_6$H$_3$.[30] The computed and experimental Ru−N$_\alpha$ distances are equal (1.81 Å), as well as the relative stereochemistry of the two imido ligands, which eclipse each other, but their plan is differently oriented with respect to the [Ru] basal unit. In the optimized model, the two NCH$_3$ ligands project halfway in between two consecutive Ru−N$_{TTP}$ bonds. However, the 45° torsion is about halved (22°) in the real structure, minimizing in this way the steric hindrance between the bulky aryl groups and the TPP phenyl substituents. As previously mentioned, the rotational freedom of apical ligands importantly affects the interactions between the metal d$_\pi$ orbitals and the nonequivalent imido p$_\pi$ ones (Scheme 3) with consequences for the electronic structure.

The formation of the singlet [Ru](NCH$_3$)$_{2\ S}$ determines the formal Ru^{IV}→Ru^{VI} oxidation with the unique metal electron pair (d^2) in the nonbonding d$_{xy}$ orbital. With reference to Scheme 3b, the two d$_\pi$ orbitals, slightly different in energy, must be vacant. Therefore, the derived triplet isomer [Ru](NCH$_3$)$_{2\ T}$ should have configuration (d$_{xy}$)^1(d$_{xz}$)^1, as also suggested by other authors for a comparable OEP complex.[44] Surprisingly, the computed wave functions, shown in the upper of Figure 7, indicate essentially equivalent α and β
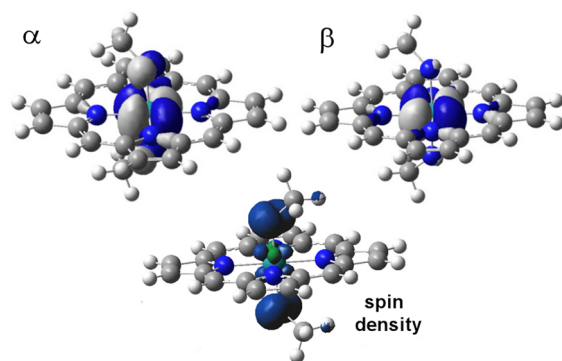

Figure 7. Upper part: equivalent α and β spin components of the d$_{xy}$ orbital in [Ru](NCH$_3$)$_{2\ T}$. Lower part: prevailing spin density at the *trans*-axial N atoms.

spins for d$_{xy}$, confirming its double population as in the singlet. Therefore, the two unpaired electrons in [Ru](NCH$_3$)$_{2\ T}$ have scarce metal character, as also emerging from the spin density plot in the lower part of Figure 7. The calculations show that the spin is mainly localized at the apical N atoms with a very small metal contribution (0.9 vs 0.02 e^2/bohr^3). As an explanation, the unpaired electrons have unique NCH$_3$ character, suggesting the partial reduction of these ligands to monoanions (NCH$_3^-$) rather then dianions.

For related iron species, such as cytochrome P450, the porphyrin p_π system was proposed to supply frontier unpaired electrons,[26] but no significant TPP spin contribution emerges from the present case (Figure 7). Although more focused studies are needed to define the precise electronic structure of $[Ru](NCH_3)_{2\,T}$, data recorded up to now confirm the diradical character of the NR ligands which fundamentally supports the catalytic activity of the system.

Radical Activation of the Substrate C−H Bond by $[Ru](NCH_3)(CO)_T$ or $[Ru](NCH_3)_{2\,T}$. The triplet states for both the mono- and bis-imido species help to understand the C−H bond activation of an organic substrate such as cyclohexene (C_6H_{10}) to afford the allylic amine $HN(C_6H_9)CH_3$ and a number of byproducts. In fact, radical mechanisms are hypothesized and supported by DFT calculations.

Reactivity of $[Ru](NCH_3)(CO)$ Monoimido Derivatives. Although never isolated, the monoimido carbonyl complex, derived from the activation of one azide molecule, plays a key role in both their singlet or triplet state. $[Ru](NCH_3)(CO)_S$ is prone to releasing the CO ligand and favoring the activation of a second azide molecule to form the bis-imido derivatives (Scheme 5). Alternatively, the somewhat more stable triplet $[Ru](NCH_3)(CO)_T$, with a diradical character (Scheme 4) at the NCH_3 ligand (Figure 5), can activate a cyclohexene C−H bond to yield the allylic amine. The corresponding energy profile is illustrated in Scheme 6.

Scheme 6. Energy Profile for the Allylic Amine Formation
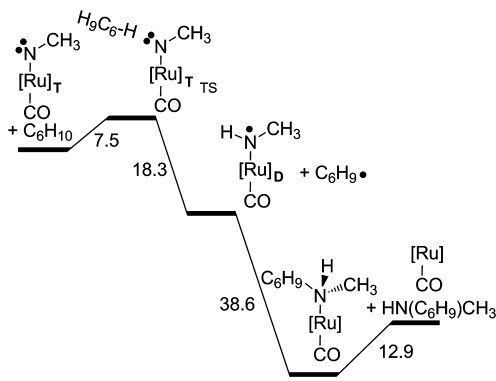
The adduct between C_6H_{10} and $[Ru](NCH_3)(CO)_T$ corresponds to the $([Ru](NCH_3)(CO)_T{*}C_6H_{10})_{TS}$ transition state with the relatively small barrier of +7.5 kcal mol^{-1}. The species, depicted in Figure 8, features the two almost collinear and somewhat elongated C−H and N−H linkages (1.25 and

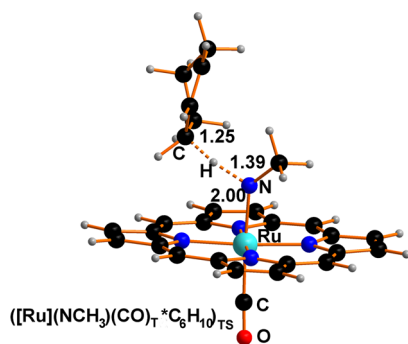**Figure 8.** Optimized $([Ru](NCH_3)(CO)_T{*}C_6H_{10})_{TS}$ structure.

1.39 Å, respectively). This suggests that one of the unpaired electrons of the coordinated nitrogen atom delocalizes toward the cyclohexene ring favoring the separation of the radical $C_6H_9{}^\bullet$ and the amido complex $[Ru](HNCH_3)(CO)_D$ in Figure S7. As shown in Scheme 6, the process is exergonic by −18.3 kcal mol^{-1}.

From a plot of the $[Ru](HNCH_3)(CO)_D$ spin density, the unpaired electron appears largely localized at the amido N atom (0.8 e^2/bohr^3), which should be treated as an uncharged radical rather than a monoanion. The $C_6H_9{}^\bullet$ species is a stable minimum thanks to the partial endocyclic delocalization over three adjacent carbon atoms of the allylic-type character.[45] Therefore, $C_6H_9{}^\bullet$ can remotely migrate to exert its radical reactivity (see below). Probably, $C_6H_9{}^\bullet$ combines with the $[Ru](HNCH_3)(CO)_D$ radical in a highly exorgeonic manner (−38.6 kcal mol^{-1}) to give the diamagnetic amino complex $[Ru](HN(C_6H_9)CH_3)(CO)$ (Figure S8). A reactivity pattern of this type is known as the "rebound mechanism," which was proposed for some metallo-porphyrin promoted oxidations.[46] In these cases, the initial H-abstraction from an R−H bond is followed by the combination of the freed R$^\bullet$ radical with the generated OH group.[47] It should be noted that the rebound mechanism was also underlined[22,24] in the case of the cobalt-promoted aminations.

The last step of the process in Scheme 6 corresponds to the release of the desired allylic amine as already deducible from the rather weak Ru−N$_{amine}$ bond of 2.36 Å of $[Ru](HN(C_6H_9)CH_3)(CO)$. Although this process costs +12.9 kcal mol^{-1}, it importantly restores the precursor $[Ru](CO)$ for a new catalytic cycle. Incidentally, the same process is exergonic by −8.4 kcal mol^{-1} at the B3LYP level, confirming the relevance of the dispersion forces in these systems.

The separation of stable doublets after TS (Scheme 6) addresses the largely debated problem of the H transfer mechanism at transition metal complexes. This has been interpreted as the combined motion of two elementary particles such as a proton and an electron.[48] Therefore, while the former is captured by a ligand having residual basicity, the latter reduces the metal atom. Our interpretation of the process, based on the intersystem crossing, instead implies that a H$^\bullet$ radical transfers to the NCH_3 group, which in the triplet complex resembles the free nitrene of Scheme 3a. In other words, H$^\bullet$ couples its electron with an unpaired one on nitrogen to form the N−H bond without affecting the metal oxidation state.

The overall amination reaction, summarized by eq 1, has the largely exorgonic balance of −44.8 kcal mol^{-1}. The formation of the allylic amine may continue as long as equimolar amounts of azide and cyclohexene are available.

$$CH_3N_3 + C_6H_{10} \xrightarrow{[Ru]CO} HN(C_6H_9)CH_3 + N_2 \qquad (1)$$
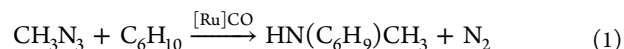
The catalytic cycle described up to now is interrupted upon the CO loss from the singlet $[Ru](NCH_3)(CO)_S$ (last step in Scheme 2). At this point, a different catalytic cycle can start with the activation of a second azide molecule giving the bis-imido isomers $[Ru](NCH_3)_{2\,S}$ and $[Ru](NCH_3)_{2\,T}$ (Scheme 5).

Reactivity of $[Ru](NCH_3)_2$ Bis-Imido Derivatives. Diamagnetic complexes of the type $[Ru](NAr)_2$ were experimentally isolated[30] and validated for their independent capability of promoting the catalytic amination of cyclohexene. Our DFT studies suggest that the triplet isomer $[Ru]$-

$(NCH_3)_{2\ T}$ is formed at a energy cost of 16.1 kcal mol^{-1} (Scheme 5) and promotes the C−H activation due to the presence of unpaired electrons at the two NCH$_3$ groups. The process likely occurs through the transition state ([Ru]-$(NCH_3)_{2\ T}*C_6H_{10})_{TS}$ analogous to the optimized ([Ru]-$(NCH_3)(CO)_T*C_6H_{10})_{TS}$ one (Figure 8). In actuality, the species could not be optimized due to the rather flat PES around it. In fact, ad-hoc scans, performed by linearly approaching one C−H bond of the substrate to the imido N atom, indicate that the barrier is at most +3 kcal mol^{-1}. It is worth mentioning that, after the original submission of this paper, other authors presented a comparable computational study for the stoichiometric amination of C−H benzylic bonds performed by the complex $[Ru](NMs)_2$ (Ms = SO$_2$-p-MeOC$_6$H$_4$).[49] In this case, a triplet TS, similar to the one expected by us, was optimized, but the authors pointed out a somewhat more favorable singlet pathway on the basis of a TS also showing a linear C···H···N arrangement. Conversely, we suggest that the first order process, leading to the distinct N−C and N−H linkages in the amine product, should involve a triangular arrangement of the three atoms, which is unaccounted for in the published[49] reaction profile. For this reason, we continue to believe that the separation of radicals after TS (hence a higher order reactivity) is more viable for systems of this type.

The analysis of the triplet PES also justifies the formation of some byproducts indicated below. In particular, Scheme 7

Scheme 7. Energy Profile for the Radical Reactivity of $[Ru](NCH_3)_{2\ T}$
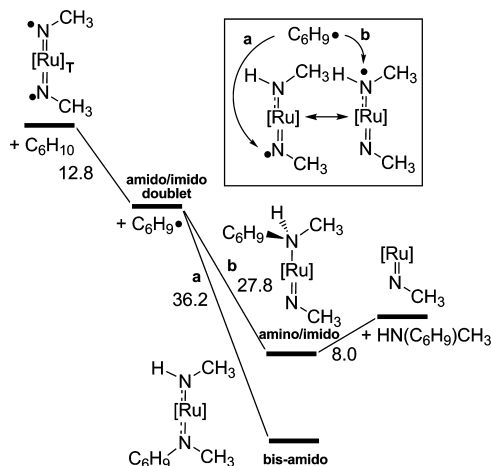
shows that the homolytic cleavage of the C−H bond, yielding the doublets $[Ru](NCH_3)(HNCH_3)_D$ (Figure S9) and C$_6$H$_9$$^\bullet$, is exergonic by −12.8 kcal mol^{-1}. Another −27.8 kcal mol^{-1} is gained upon the subsequent coupling of the two radicals (*path b* in the box of Scheme 7) to give the diamagnetic complex $[Ru](NCH_3)(HN(C_6H_9)CH_3)$ of Figure 9.

Here, the large Ru−N$_{amine}$ distance of 2.47 Å anticipates an easy amine departure, although the process costs +8.0 kcal mol^{-1}, which are again necessary to win the dispersion forces.

The release of the allylic amine leads to the known five coordinated monoimido complex $[Ru](NCH_3)_S$, which can react with another azide molecule (Scheme 5) to initiate a new catalytic cycle involving the bis-imido species. The spin density plot in Figure 10 for the imido-amino intermediate [Ru]-$(NCH_3)(HNCH_3)_D$ indicates scarce metal localization (+0.2
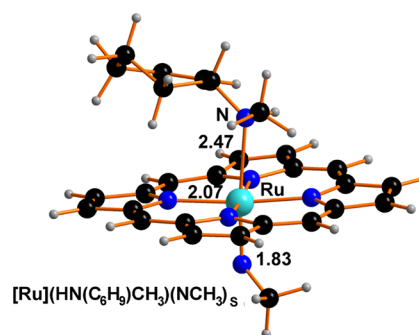

Figure 9. Optimized $[Ru](HN(C_6H_9)CH_3)(NCH_3)_S$ structure.

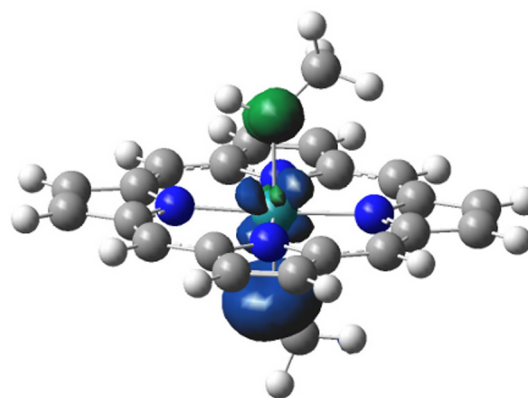**Figure 10.** Spin density distribution in$[Ru](NCH_3)(HNCH_3)_D$.

e^2/bohr^3), while larger values of the opposite sign are computed for the imido and amido N atoms (+1.13 and −0.43 e^2/bohr^3, respectively). Although the spin concentration at the amido ligand suggests poor coupling capabilities, the allylic amine is likely formed when C$_6$H$_9$$^\bullet$ is still in close proximity. Conversely, the radical migration may allow either inter- or intramolecular coupling. In the latter case, the $[Ru](N(C_6H_9)CH_3)(HNCH_3)_S$ complex with different diamido ligands (Figure S10) forms as the deepest minimum of Scheme 7 (*path a* in the box) with a ΔG gain of −36.2 kcal mol^{-1}. On the other hand, intermolecular migrations lead to alternative bis-amido complexes (see SI), which can be indicated as byproducts or resting intermediates. The latter attribution ensues from the radical catalytic reactivity observed in some cases, possibly due to an accessible intersystem crossing. Such a subject will be analyzed in detail in a future publication, although the formation of a bis-amido triplet is addressed below to justify the formation of a dimeric $[Ru]_2$ byproduct.

Importantly, the five-coordinated singlets $[Ru](CO)_S$ and $[Ru](NCH_3)_S$ similarly allow the activation of one azide molecule and the continuation of the respective catalytic cycles through a radical mechanism in which cyclohexene is aminated (Scheme 1). The overall process based on the bis-imido species $[Ru](NCH_3)_{2\ S}$ (eq 2) has practically the same exergonicity of that illustrated in eq 1 (−44.8 and −44.4 kcal mol^{-1}, respectively). However, the most critical point in the two processes has a different nature. In the amination promoted by $[Ru](CO)_S$, the highest barrier corresponds to the activation of the azide (+26.8 kcal mol^{-1}, Scheme 2), while the intersystem crossing step is the most expensive one for the amination catalyzed by $[Ru](NCH_3)_S$ (+16.1 kcal mol^{-1}, Scheme 5).

$$CH_3N_3 + C_6H_{10} \xrightarrow{[Ru](NCH_3)_{2\,S}} HN(C_6H_9)CH_3 + N_2 \qquad (2)$$
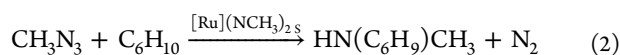
These computational results strongly support the experimental and kinetics studies,[20] which already suggested the existence of two interconnected catalytic cycles without providing a clear-cut distinction between them.

Byproducts or Resting Intermediates. As previously reported, the catalyst $[Ru](NAr)_{2\,S}$ can be the precursor of mixed bis-amido complexes such as $[Ru](N(C_6H_9)Ar)(HNAr)$ and analogous species with equal pairs of *trans* amido ligands such as HNAr or $N(C_6H_9)Ar$. The optimized models are shown in Figures S11 and S12, respectively, and a discussion on their possible formation is also provided in an SI section. Other detected byproducts are $C_{12}H_{18}$ deriving from the C−C coupling of two allylic C_6H_9 radicals and a black amorphous compound, which probably corresponds to the known dimer $[Ru]_2$ complex.

The Paramagnetic $[Ru]_2$ Dimer Complex. The NMR spectroscopy of a crude catalytic mixture revealed the presence of a black paramagnetic species,[50] which was hypothesized to be the X-ray characterized double-decker $[Ru]_2$.[51] Our unprecedented full optimization of the $[Ru]_2$ triplet (Figure 11) confirms the short Ru−Ru experimental distance of 2.34 Å

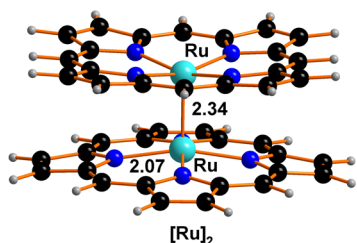**Figure 11.** Optimized structure of $[Ru]_2$ in triplet configuration.

in accordance with the existence of a double bond as already proposed by a qualitative MO explanation reported in the original paper.[51]

Namely, the two Ru^{II} ions have four nonbonding electrons, while the other eight are involved in direct σ and π interactions. Given the population of the bonding σ level, the remaining six electrons occupy the d_π−d_π bonding and antibonding "e" degenerate sets, with the higher one characterized by two unpaired spins. Therefore, two Ru−Ru half π-bonds are present besides the σ one. The original paper indicated that the synthesis of $[Ru]_2$ occurs through the pyrolysis of the mononuclear complex $[Ru](pyridine)_2$.[51] Thus, after the loss of one apical ligand, two five-coordinate fragments would dimerize with the ultimate departure of the still coordinated pyridine ligand. By analogy, our $[Ru]_2$ precursor can be the byproduct $[Ru](HN(C_6H_9)CH_3)_2$ derived from a double C−H activation performed by the bis-amido species $[Ru](N(C_6H_9)-CH_3)_2$ to also provide that this species can exist as a triplet. As a matter of fact, the black residue was experimentally observed during the amination catalysis promoted by the isolated singlet $[Ru](N(C_6H_9)Ar)_{2\,S}$.[20,30]

The present theoretical studies confirm that the bis-amido model $[Ru](HNCH_3)_{2\,S}$ is −7.4 kcal mol^{-1} more stable than the triplet $[Ru](HNCH_3)_{2\,T}$ (the two isomers are shown in the Figures S11 and S13, respectively). It appears that in the triplet the two amido ligands are orthogonally oriented at variance with the coplanar arrangement present in the singlet isomer. Therefore, the torsion is the evident governing parameter of the

intersystem crossing, which occurs at a torsion angle value of 76°. The associated MECP value <1 kcal mol^{-1} confirms the feasibility of this process. The spin density plot for $[Ru]-(HNCH_3)_{2\,T}$ (Figure 12) shows equivalent distribution at the
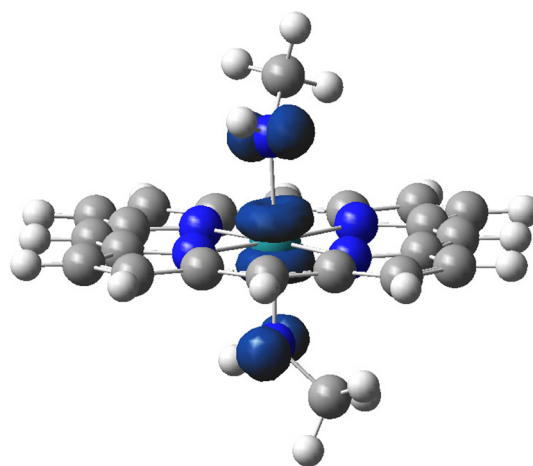
Figure 12. Spin-density distribution for the bis-amido triplet $[Ru](HNCH_3)_{2\,T}$.

metal and the N atoms (0.6 and 0.7 e^2/bohr^3, respectively), not excluding that the C−H bond of the C_6H_{10} substrate can be activated similarly to what described for bis-imido species (Scheme 7).

The formation of an amino/amido doublet ($\Delta G = -3.9$ kcal mol^{-1}) precedes that of the unsymmetrical bis-amine derivative $[Ru](H_2NR)(HN(C_6H_9)R)$ ($\Delta G = -25.8$ kcal mol^{-1}) which, after the release of the amines, leads to the paramagnetic $[Ru]_2$ byproduct. The whole process, summarized in eq 3, has a ΔE balance of −32.4 kcal mol^{-1}.[52]

$$2[Ru](HNCH_3)_T + 2C_6H_{10}$$
$$\rightarrow [Ru_2]_T + 2HN(C_6H_9)CH_3 + 2H_2NCH_3 \qquad (3)$$
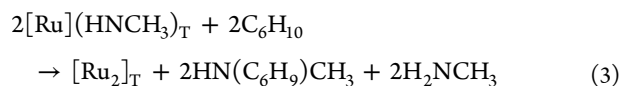
## ◼ CONCLUDING REMARKS

The computational analysis of the azide activation and amination of a cyclohexene C−H bond promoted by a $[Ru]$-based catalyst has provided mechanistic insights. The interconnection of two distinct catalytic cycles, giving the same allylic amine, has been highlighted (Scheme 8). Remarkably, both cycles are largely favored from the energy viewpoint (about −45 kcal mol^{-1}).

When $[Ru](CO)$ is involved, the N_2 departure from an anchored azide molecule leads to the singlet monoimido derivative $[Ru](CO)(NCH_3)_S$. This can either lose CO to pass to the right side cycle or be transformed into the triplet isomer $[Ru](CO)(NCH_3)_T$, which triggers the radical reactivity on the left side of Scheme 8. The spin density at the imido nitrogen atom promotes the C−H homolysis of the cyclohexene substrate with the immediate H$^\bullet$ coupling and $C_6H_9^\bullet$ release. By assuming that the latter radical remains in close proximity to the amido group (also a radical), the desired allylic amine product is generated via the known "rebound" mechanism.[46] Conversely, upon the loss of the CO ligand from the singlet $[Ru](NCH_3)(CO)_S$ (Scheme 2), a second azide molecule is anchored at the vacated site and then activated to give a bis-imido complex. The latter can also exist in distinct spin isomers,

Scheme 8. Proposed Mechanisms of C−H Amination, As Emerging from the DFT Study

catalysis over [Ru](CO)   catalysis over [Ru](NR)₂
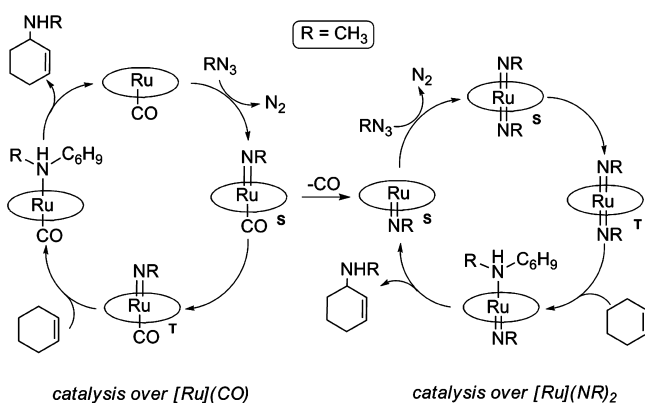
and the triplet $[Ru](NCH_3)_{2\ T}$ plays a fundamental role for the radical catalysis, since the "rebound" mechanism of C_6H_{10} over one imido ligand affords the allylic amine. On the other hand, the radical character of the *trans* imido ligands is responsible for the formation of a variety of bis-amido complexes (Scheme 7 and SI) as either byproducts or resting states displaying radical reactivity. An example of the latter behavior is the formation of the bis-amino Ru^{II} byproduct, which is proposed to be the precursor of the known paramagnetic $[Ru]_2$ double-decker (Figure 11).

The most important result from our computational analysis is that the amination chemistry by organic azides involves an intersystem crossing at the ruthenium catalyst. This theoretical interpretation has been validated by a number of experimental observations. The inhibition of catalytic reactions performed in the presence of the radical-trap TEMPO (2,2,6,6-tetramethyl-piperidin-1-yl)oxyl)[53] supports the formation of radical intermediates which can also justify the observed mixture of catalytic byproducts.

In the singlet chemistry, the formation of mono- and bis-imido derivatives implies formal metal oxidations ($Ru^{II} \rightarrow Ru^{IV}$ and $Ru^{IV} \rightarrow Ru^{VI}$, respectively), which are associated with the full nitrogen reduction (RN^{2-} dianion). However, in the corresponding triplet isomers, the NR group contains unpaired spins excluding a correspondingly high metal oxidation state. Therefore, the radical reactivity implies alternative concepts of the electron transfer.

■ COMPUTATIONAL DETAILS

The models were first optimized at the B3LYP-DFT[32] level of theory and later with the B97D[31] functional within the Gaussian 09 program.[54] All the optimized structures were validated as minima and/or transition states by computed vibrational frequencies, with the exception of $[Ru](N(C_6H_9)-CH_3)_{2\ S}$ and $[Ru]_2$ due to the lack of adequate computing power. Some selected structures have also been investigated with the BP86 functional[41] mainly with the purpose of understanding the factors for the intersystem crossing, which is a fundamental aspect of this study. All the calculations were based on the CPCM model[55] for the benzene solvent used in the experiments. The effective Stuttgart/Dresden core potential (SDD)[56] was adopted for the ruthenium atom, while for all the other atoms the basis set was 6-31G, with the addition of the polarization functions (d, p). Qualitative MO arguments have been developed with the help of the EHMO analysis of the wave functions, derived from the CACAO package[57] and

sufficiently consistent with the DFT ones. The coordinates of all the optimized structures are reported in the Supporting Information.

■ ASSOCIATED CONTENT

ⓢ Supporting Information

Tables list the Cartesian coordinates and thermal parameters of all the optimized structures. This material is available free of charge via the Internet at http://pubs.acs.org

■ AUTHOR INFORMATION

Corresponding Authors
*E-mail: gabriele.manca@iccom.cnr.it.
*E-mail: emma.gallo@unimi.it.
Notes
The authors declare no competing financial interest

■ REFERENCES

(1) Davies, H. M. L.; Manning, J. R. *Nature* **2008**, *451*, 417−424.
(2) Diaz-Requejo, M. M.; Perez, P. J. *Chem. Rev.* **2008**, *108*, 3379−3394.
(3) Collet, F.; Lescot, C.; Dauban, P. *Chem. Soc. Rev.* **2011**, *40*, 1926−1936.
(4) Minozzi, M.; Nanni, D.; Spagnolo, P. *Chem.—Eur. J.* **2009**, *15*, 7830−7840.
(5) Collet, F.; Dodd, R. H.; Dauban, P. *Chem. Commun.* **2009**, 5061−5074.
(6) Cenini, S.; Gallo, E.; Caselli, A.; Ragaini, F.; Fantauzzi, S.; Piangiolino, C. *Coord. Chem. Rev.* **2006**, *250*, 1234−1253.
(7) Bräse, S.; Gil, C.; Knepper, K.; Zimmermann, V. *Angew. Chem., Int. Ed. Engl.* **2005**, *44*, 5188−5240.
(8) Bräse, S.; Banert, K. *Organic Azides Syntheses and Applications*; John Wiley & Sons Ltd.: New York, 2010.
(9) Chiba, S. *Synlett* **2012**, *2012*, 21−44.
(10) Jung, N.; Bräse, S. *Angew. Chem., Int. Ed. Engl.* **2012**, *51*, 5538−5540.
(11) Driver, T. G. *Org. Biomol. Chem.* **2010**, *8*, 3831−3846.
(12) Xiao, J.; Deng, L. *Dalton Trans.* **2013**, *42*, 5607−5610.
(13) Nguyen, Q.; Nguyen, T.; Driver, T. G. *J. Am. Chem. Soc.* **2013**, *135*, 620−623.
(14) King, E. R.; Hennessy, E. T.; Betley, T. A. *J. Am. Chem. Soc.* **2011**, *133*, 4917−4923.
(15) Nguyen, Q.; Sun, K.; Driver, T. G. *J. Am. Chem. Soc.* **2012**, *134*, 7262−7265.
(16) Fantauzzi, S.; Caselli, A.; Gallo, E. *Dalton Trans.* **2009**, 5434−5443.
(17) Lu, H.; Zhang, X. P. *Chem. Soc. Rev.* **2011**, *40*, 1899−1909.
(18) Che, C.-M.; Lo, V. K.-Y.; Zhou, C.-Y.; Huang, J.-S. *Chem. Soc. Rev.* **2011**, *40*, 1950−1975.
(19) Liu, Y.; Che, C.-M. *Chem.—Eur. J.* **2010**, *16*, 10494−10501.
(20) Intrieri, D.; Caselli, A.; Ragaini, F.; Macchi, P.; Casati, N.; Gallo, E. *Eur. J. Inorg. Chem.* **2012**, 569−580.
(21) Suarez, A. I. O.; Jiang, H.; Zhang, X. P.; de Bruin, B. *Dalton Trans.* **2011**, *40*, 5697−5705.
(22) Lyaskovskyy, V.; Suarez, A. I. O.; Lu, H.; Jiang, H.; Zhang, X. P.; de Bruin, B. *J. Am. Chem. Soc.* **2011**, *133*, 12264−12273.
(23) Lu, H.; Jiang, H.; Hu, Y.; Wojtas, L.; Zhang, X. P. *Chem. Sci.* **2011**, *2*, 2361−2366.
(24) Hopmann, K. H.; Ghosh, A. *ACS Catal.* **2011**, *1*, 597−600.

(25) Caselli, A.; Gallo, E.; Fantauzzi, S.; Morlacchi, S.; Ragaini, F.; Cenini, S. *Eur. J. Inorg. Chem.* **2008**, 3009−3019.

(26) Moreau, Y.; Chen, H.; Derat, E.; Hirao, H.; Bolm, C.; Shaik, S. *J. Phys. Chem. B* **2007**, 111, 10288−10299.

(27) Leung, S. K.-Y.; Tsui, W.-M.; Huang, J.-S.; Che, C.-M.; Liang, J.-L.; Zhu, N. *J. Am. Chem. Soc.* **2005**, 127, 16629−16640.

(28) Ragaini, F.; Penoni, A.; Gallo, E.; Tollari, S.; Gotti, C. L.; Lapadula, M.; Mangioni, E.; Cenini, S. *Chem.—Eur. J.* **2003**, 9, 249−259.

(29) Musaev, D. G.; Blakey, S. B. *Organometallics* **2012**, 31, 4950−4961.

(30) Fantauzzi, S.; Gallo, E.; Caselli, A.; Ragaini, F.; Casati, N.; Macchi, P.; Cenini, S. *Chem. Commun.* **2009**, 3952−3954.

(31) Grimme, S. *J. Chem. Phys.* **2006**, 124, 34108−35124.

(32) Becke, A. D. *J. Chem. Phys.* **1993**, 98, 5648−5652.

(33) *Cambridge Structural Database System*, version 5.32; Cambridge Crystallographic Data Centre: Cambridge, U. K.

(34) Gallo, E.; Caselli, A.; Ragaini, F.; Fantauzzi, S.; Masciocchi, N.; Sironi, A.; Cenini, S. *Inorg. Chem.* **2005**, 44, 2039−2049.

(35) Ishii, T.; Aizawa, N.; Yamashita, M.; Matsuzaka, H.; Kodama, T.; Kikuchi, K.; Ikemoto, I.; Iwasa, Y. *J. Chem. Soc., Dalton Trans.* **2000**, 4407−4412.

(36) Lamberti, M.; Fortman, G. C.; Poater, A.; Broggi, J.; Slawin, A. M. Z.; Cavallo, L.; Nolan, S. P. *Organometallics* **2012**, 31, 756−767.

(37) Boren, B. C.; Narayan, S.; Rasmussen, L. K.; Zhang, L.; Zhao, H.; Lin, Z.; Jia, G.; Fokin, V. V. *J. Am. Chem. Soc.* **2008**, 130, 8923−8930.

(38) Proulx, G.; Bergman, R. G. *J. Am. Chem. Soc.* **1995**, 117, 6382−6383.

(39) (a) Nishigaki, J.; Matsumoto, T.; Tatsumi, K. *Inorg. Chem.* **2012**, 51, 5173−5187. (b) Nishigaki, J.; Matsumoto, T.; Manca, G.; Mealli, C.; Tatsumi, K. Unpublished results. Presented as a poster at Roald Hoffmann's 75th Birthday Symposium July 21−22, 2012, Cornell University, Ithaca, NY.

(40) Aryl azides with electron withdrawing florurate substituents on the aryl moiety are typically used for their high stability/reactivity relationship.

(41) (a) Becke, A. D. *Phys. Rev. A* **1988**, 38, 3098−3100. (b) Perdew, J. P. *Phys. Rev. B* **1986**, 33, 8822−8824.

(42) (a) Harvey, J. N.; Poli, R.; Smith, K. M. *Coord. Chem. Rev.* **2003**, 238−239, 347−361. (b) Harvey, J. N.; Aschi, M. *Farad. Discussion* **2003**, 124, 129−143.

(43) Borden, W. T.; Gritsan, N. P.; Karney, W. L.; Kemnitz, C. R.; Platz, M. S. *Acc. Chem. Res.* **2000**, 33, 765−771.

(44) Zdilla, M. J.; Abu-Omar, M. M. *J. Am. Chem. Soc.* **2006**, 128, 16971−16979.

(45) (a) Fleming, I. *Molecular Orbitals and Organic Chemical Reactions*: John Wiley and Sons, 2009; 22−28. (b) McMurry, J. *Organic Chemistry*; Brooks/Cole Pub Co, 1999; pp 365−366.

(46) Groves, J. T. *J. Chem. Educ.* **1985**, 26, 928−931.

(47) Balcells, D.; Raynaud, C.; Crabtree, R. H.; Eisenstein, O. *Chem.Comm.* **2009**, 1772−1174.

(48) Mayer, J. M. *Acc. Chem. Res.* **2011**, 44, 36−46.

(49) Guo, Z.; Guan, X.; Huang, J.-S.; Tsui, W.-M.; Lin, Z.; Che, C.-M. *Chem.—Eur. J.* **2013**, 19, 11320−11331.

(50) The NMR spectrum of a catalytic residue in C_6D_6 showed the presence of typical paramagnetic signals at +17.14, −21.55, −30.08, and −32.69 ppm. Unfortunately, the purification of the catalytic mixture did not afford any pure compound.

(51) Collman, J. P.; Barnes, C. E.; Swepston, P. N.; Ibers, J. A. *J. Am. Chem. Soc.* **1984**, 106, 3500−3510.

(52) Computational limitations did not allow calculation of the frequencies for the optimized $[Ru]_2$, hence the energetics of reaction cannot be expressed in ΔG terms.

(53) Lebelev, O. L.; Kazarnovskii, S. N. *Zhur. Obshch. Khim.* **1960**, 30, 1631.

(54) Frisch, M. J.; Trucks, G. W.; Schlegel, H. B.; Scuseria, G. E.; Robb, M. A.; Cheeseman, J. R.; Scalmani, G.; Barone, V.; Mennucci, B.; Petersson, G. A.; Nakatsuji, H.; Caricato, M.; Li, X.; Hratchian, H.

P.; Izmaylov, A. F.; Bloino, J.; Zheng, G.; Sonnenberg, J. L.; Hada, M.; Ehara, M.; Toyota, K.; Fukuda, R.; Hasegawa, J.; Ishida, M.; Nakajima, T.; Honda, Y.; Kitao, O.; Nakai, H.; Vreven, T.; Montgomery, J. A., Jr.; Peralta, J. E.; Ogliaro, F.; Bearpark, M.; Heyd, J. J.; Brothers, E.; Kudin, K. N.; Staroverov, V. N.; Kobayashi, R.; Normand, J.; Raghavachari, K.; Rendell, A.; Burant, J. C.; Iyengar, S. S.; Tomasi, J.; Cossi, M.; Rega, N.; Millam, J. M.; Klene, M.; Knox, J. E.; Cross, J. B.; Bakken, V.; Adamo, C.; Jaramillo, J.; Gomperts, R.; Stratmann, R. E.; Yazyev, O.; Austin, A. J.; Cammi, R.; Pomelli, C.; Ochterski, J. W.; Martin, R. L.; Morokuma, K.; Zakrzewski, V. G.; Voth, G. A.; Salvador, P.; Dannenberg, J. J.; Dapprich, S.; Daniels, A. D.; Farkas, Ö.; Foresman, J. B.; Ortiz, J. V.; Cioslowski, J.; Fox, D. J. *Gaussian 0.9*, revision B.01; Gaussian, Inc.: Wallingford, CT, 2010.

(55) (a) Barone, V.; Cossi, M. *J. Phys. Chem. A* **1998**, 102, 1995−2001. (b) Cossi, M.; Rega, N.; Scalmani, G.; Barone, V. *J. Comput. Chem.* **2003**, 24, 669−681.

(56) Dolg, M.; Stoll, H.; Preuss, H.; Pitzer, R. M. *J. Phys. Chem.* **1993**, 97, 5852−5859.

(57) (a) Mealli, C.; Proserpio, D. M. *J. Chem. Educ.* **1990**, 67, 399. (b) Mealli, C.; Ienco, A.; Proserpio, D. M. *Book of Abstracts of the XXXIII ICCC*; Ed. CNR, Area della Ricerca di Firenze: Florence, 1998; p 510.